Research Article Vol. 29, No. 4 / 15 February 2021 / Optics Express 6053
Optics EXPRESS

High-precision cavity spectroscopy using high-frequency squeezed light

JONAS JUNKER,[1,*] DENNIS WILKEN,[1] ELANOR HUNTINGTON,[2] AND MICHÈLE HEURS[1]

[1]Max Planck Institute for Gravitational Physics (Albert Einstein Institute), and Institute for Gravitational Physics, Leibniz Universität Hannover, Callinstrße 38, 30167 Hannover, Germany
[2]Centre for Quantum Computation & Communication Technology and Research School of Engineering, The Australian National University, Canberra, ACT 2601, Australia
[*]jonas.junker@aei.mpg.de

Abstract: In this article, we present a novel spectroscopy technique that improves the signal-to-shot-noise ratio without the need to increase the laser power. Detrimental effects by technical noise sources are avoided by frequency-modulation techniques (frequency up-shifting). Superimposing the signal on non-classical states of light leads to a reduced quantum noise floor. Our method reveals in a proof-of-concept experiment small signals at Hz to kHz frequencies even below the shot noise limit. Our theoretical calculations fully support our experimental findings. The proposed technique is interesting for applications such as high-precision cavity spectroscopy, e.g., for explosive trace gas detection where the specific gas might set an upper limit for the laser power employed.

1. Introduction

Successful blue-sky experiments, such as the first direct detection of gravitational waves (GWs) in 2015 [1] require an intimidatingly high measurement sensitivity. In a GW detector the signal originates from the relative differential distance change caused by a GW, as measurable with a Michelson-type interferometer [1]. In this particular case of the GW event GW150914 a strain sensitivity of $\Delta L/L \approx 10^{-23}$ was required. Other types of high-precision metrology experiments detect other types of signals, but they have one requirement in common: All call for high sensitivity and detection with a sufficiently large signal-to-noise ratio (SNR).

As an example, in laser absorption spectroscopy [2,3] the concentration of a gas phase can be determined by measuring the interaction of a laser field with the gas molecules. The challenge here often lies in the fact that the spectroscopic signal to be detected is inordinately small - this makes its detection inherently difficult, but it additionally makes the signal highly susceptible to noise. These challenges can be generalized to the detection of any small signal.

The obvious way to maximize the SNR is to increase the signal and to decrease the noise. At low measurement frequencies, active feedback control often serves to suppress the dominant technical noise sources down to the fundamental shot noise limit [4–7]. In addition to noise reduction, the achieved signal-to-shot-noise ratio can be improved by increasing the laser power, as relative shot noise falls with the square root of the laser power.

In spectroscopic applications, amplifying the laser power increases the interaction strength and hence amplifies the signal. In some cases, however, the signal strength cannot be increased: for technical reasons such as damage thresholds [8,9], or for fundamental reasons, e.g. if the origin of the signal is astrophysical [10]. In other cases, the intrinsic noise of the measurement apparatus is already governed by quantum shot noise, making a further reduction of the noise floor seem initially unfeasible.

Technical noise is always present in experiments, in particular at low measurement frequencies in the Hz and kHz regions. Typical examples of technical noise sources include seismic noise

#416713 https://doi.org/10.1364/OE.416713
Journal © 2021 Received 9 Dec 2020; revised 15 Jan 2021; accepted 15 Jan 2021; published 10 Feb 2021

Optics EXPRESS

and mechanical vibrations, electronic noise, laser intensity and frequency noise, or fluctuations of air currents leading to variations in the index of refraction of the air through which light propagates. In principle, technical noise sources can be suppressed to arbitrarily low noise levels, depending on the time, effort, energy, cost, and corresponding technical sophistication invested in the experimental setup. Quantum noise, however, poses a more fundamental limit, which is expressed in the Heisenberg Uncertainty Relation. Quantum shot noise occurring in laser experiments originates from the Poissonian photon statistics of the coherent state [11], which is emitted by a technically well-stabilized laser.

The application of squeezed light [12] can reduce the relative shot noise and thus improve the SNR [13–15]. In this regard it acts like an increase in laser power, but without the drawbacks associated with higher optical power, such as increased absorption, higher thermal load, excess scattering, etc. Squeezed light first was experimentally demonstrated in 1985 [16] and has gained increasing relevance over the last decades. While the first squeezing experiment reduced the shot noise only by 0.3 dB, the highest achieved squeezing level to date lies at more than 15 dB [17]. The number of possible applications is too numerous to list, ranging from GW detection [14] over continuous variable quantum computing [18] to quantum imaging [19,20] and teleportation [21,22]. Squeezing generated at low frequencies (LFs) [23,24] always comes at the cost of considerable technical effort; in comparison, high-frequency (HF) squeezing [25–27] can drastically reduce these efforts.

Squeezing at base-band has been utilized to improve spectroscopic measurements [28,29], e.g. on atomic cesium [30]. Recently, a quantum enhancement of the SNR of 3.6 dB relative to the shot noise limited SNR was demonstrated in stimulated Raman spectroscopy [31]. In these experiments [28–31], a squeezed probe beam was transmitted through samples and then detected. However, an even higher signal strength can be achieved by enhancing the probe field in an optical resonator.

In this paper, we show in a proof-of-concept experiment the application of HF squeezing for cavity enhanced phase-sensitive spectroscopy. We report on a novel method that circumvents technical noise sources and improves the SNR without the need to increase the laser power and enables more advanced techniques such as noise-immune cavity-enhanced optical-heterodyne molecular spectroscopy (NICE-OHMS) [32]. We benefit from the advantages of HF squeezing by shifting the signal of interest (at Hz or kHz frequencies) to 200 MHz. We apply a small cavity length modulation as a signal that would conventionally be masked by quantum shot noise at HF. With our approach this signal can be revealed in a 6 dB squeezed noise floor. The results of our research are very promising for applications in high-precision metrology as in quantum spectroscopy, in particular for frequency modulation spectroscopy (FMS) [33] or trace gas detection [34,35] where the potentially explosive gas sets an upper limit for the employed laser power.

In Sec. II we provide a theoretical description of the effect of a cavity length modulation on a phase modulated laser field. We derive the variances, if the modulated field's amplitude quadrature is squeezed in an optical parametric oscillator (OPO) before it senses the cavity length modulation. Sec. III gives a detailed description of our experimental setup. In Sec. IV we present our results including the measurements that show cavity length modulation signals in the reduced noise floor around 200 MHz. In Sec. V we discuss our results, identify drawbacks and benefits of our method and give a brief outlook. We end with a conclusion in Sec. VI.

2. Theory

We detect artificial length variations of a cavity that are generated with a piezoelectric actuator at LFs. If we send a probe field through this cavity, a phase modulation (PM) is imprinted on the field that can be detected in transmission. In this section, we first calculate the variance of such a field. Second, we look at the case of a probe field that is phase modulated at the free spectral

Optics EXPRESS

range (FSR)-frequency. Third, we determine the output variance when using a probe field that is additionally squeezed. This allows an improvement of the SNR, when the classical measurement was shot-noise-limited.

2.1. Detecting a cavity length modulation

We start with the simple case of a Fabry-Perot (FP) cavity shown in Fig. 1. From the left, a classical laser field $\hat{A}_{\mathrm{in}}$ is sent into the impedance matched cavity with two loss-less mirrors with equal reflectivities R and detuning Δ. We want to determine the output field $\hat{A}_{\mathrm{out}}$ in transmission.

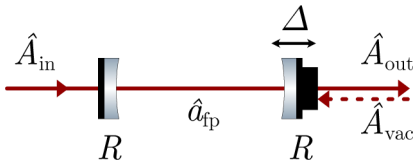

Fig. 1. Schematic of the length modulated FP cavity.

For the calculations we are following the approach in [11]. We can express the circulating cavity mode amplitude $\hat{a}_{\mathrm{fp}}$ after one cavity round-trip time τ_{fp} by

$$\hat{a}_{\mathrm{fp}}(t+\tau_{\mathrm{fp}}) = \exp(i\Delta)\Big(R\hat{a}_{\mathrm{fp}}(t) + \sqrt{T\tau_{\mathrm{fp}}}\big(\hat{A}_{\mathrm{in}}(t) + \hat{A}_{\mathrm{vac}}(t)\big)\Big). \tag{1}$$

The circulating mode amplitude after one cavity round-trip time depends on the initially circulating mode $\hat{a}_{\mathrm{fp}}(t)$ and on the two input rates $\hat{A}_{\mathrm{in}}(t)$ and $\hat{A}_{\mathrm{vac}}(t)$. Next, we consider the cavity length modulation as phase modulation for the intra-cavity field. Therefore, we set $\Delta = d\sin(\omega_{\mathrm{s}}t)$ where ω_{s} is the modulation frequency. After separating DC and fluctuating terms with $\hat{a}(t) = \bar{a} + \delta\hat{a}(t)$ and linearizing then, we can focus on the fluctuating part of Eq. (1) and find that

$$\begin{aligned}\delta\hat{a}_{\mathrm{fp}}(t+\tau_{\mathrm{fp}}) = -\bar{a}_{\mathrm{fp}}\Big(1 - \exp(id\sin(\omega_{\mathrm{s}}t))\Big)\\ + \exp(id\sin(\omega_{\mathrm{s}}t))\Big(\sqrt{T\tau_{\mathrm{fp}}}\big(\delta\hat{A}_{\mathrm{in}}(t) + \delta\hat{A}_{\mathrm{vac}}(t)\big) + R\delta\hat{a}_{\mathrm{fp}}(t)\Big)\end{aligned} \tag{2}$$

The exponential expressions in Eq. (2) can be approximated using Bessel functions of the first kind. For small cavity length changes $d \ll 1$ we can approximate

$$\exp(id\sin(\omega_{\mathrm{s}}t)) \approx 1 + \frac{d}{2}\Big(\exp(i\omega_{\mathrm{s}}t) - \exp(-i\omega_{\mathrm{s}}t)\Big) \tag{3}$$

and call the $\exp(\pm i\omega_{\mathrm{s}}t)$ terms sidebands. Next, we can transform Eq. (2) to Fourier space analog to [25] by substituting $\hat{a}(t+\tau) \rightleftharpoons \tilde{a}(\omega)\exp(i\omega\tau)$. We can solve for the fluctuating part

$$\delta\tilde{a}_{\mathrm{fp}}(\omega) = \frac{2(\delta\tilde{A}_{\mathrm{in}} + \delta\tilde{A}_{\mathrm{vac}})\sqrt{T\tau_{\mathrm{fp}}} + \bar{a}_{\mathrm{fp}}d(\delta_{\omega+\omega_{\mathrm{s}}} - \delta_{\omega-\omega_{\mathrm{s}}})}{2(\exp(i\tau_{\mathrm{fp}}\omega) - R)}. \tag{4}$$

The cavity length modulation sidebands are now represented by the Dirac delta functions $\delta_{\omega\pm\omega_{\mathrm{s}}} := \delta(\omega \pm \omega_{\mathrm{s}})$, both scaling with the modulation amplitude d and with the cavity mean field $\bar{a}_{\mathrm{fp}}$.

Optics EXPRESS

We use the input-output theory from [36], including the quantum boundary conditions, to derive the field fluctuations leaving the FP cavity as

$$\delta\tilde{A}_{\mathrm{out,fp}} = \sqrt{T/\tau_{\mathrm{fp}}}\delta\tilde{a}_{\mathrm{fp}} - \sqrt{R}\delta\tilde{A}_{\mathrm{vac}}. \tag{5}$$

If we detect the output field, we can measure the amplitude (+) or phase quadrature (-) fluctuations

$$\delta\tilde{X}^{+}(\omega) = \delta\tilde{A}(\omega) + \delta\tilde{A}(-\omega)^{\dagger}, \tag{6}$$

$$\delta\tilde{X}^{-}(\omega) = i\big(\delta\tilde{A}(\omega) - \delta\tilde{A}(-\omega)^{\dagger}\big), \tag{7}$$

where $\delta\tilde{a}^{\dagger}(\omega) = \delta\tilde{a}(-\omega)^{\dagger}$ [37]. Finally, we are interested in the variances $V^{\pm}(\omega) = \left\langle|\delta\tilde{X}^{\pm}(\omega)|^2\right\rangle$. Since the Dirac delta function δ is only an idealization and its square is not defined mathematically, below we replace them by Dirac delta-like functions $\tilde{\delta}$ with finite width, which are later defined in Eq. (23). Physically, the width of those sidebands corresponds to the technical noise present in the modulation sidebands. Assuming uncorrelated input fields $\tilde{A}_{\mathrm{vac}}$ and $\tilde{A}_{\mathrm{in}}$, the output variances read

$$V^{+}_{\mathrm{fp}}(\omega) = \big|A(\omega)\big|^2 V^{+}_{\mathrm{in}}(\omega) + \big|B(\omega)\big|^2 V^{+}_{\mathrm{vac}}(\omega) + V^{+}_{\mathrm{n}}(\omega), \tag{8}$$

$$\begin{aligned} V^{-}_{\mathrm{fp}}(\omega) = {} & \big|A(\omega)\big|^2 V^{-}_{\mathrm{in}}(\omega) + \big|B(\omega)\big|^2 V^{-}_{\mathrm{vac}}(\omega) \\ & + \left|\frac{i\bar{a}_{\mathrm{fp}} d\sqrt{T}}{\sqrt{\tau_{\mathrm{fp}}}(\exp(i\tau_{\mathrm{fp}}\omega) - R)}(\tilde{\delta}_{\omega+\omega_{\mathrm{s}}} - \tilde{\delta}_{\omega-\omega_{\mathrm{s}}})\right|^2 + V^{-}_{\mathrm{n}}(\omega), \end{aligned} \tag{9}$$

where $A(\omega)$ and $B(\omega)$ are cavity related pre-factors specified as

$$A(\omega) = \frac{T}{\exp(i\tau_{\mathrm{fp}}\omega) - R} \tag{10}$$

$$B(\omega) = -\sqrt{R} + \frac{T}{\exp(i\tau_{\mathrm{fp}}\omega) - R}. \tag{11}$$

Evidently, the two sidebands oscillating with $\omega \pm \omega_{\mathrm{s}}$ originate from the cavity length modulation. They will only appear in the phase quadrature output variance V^{-}_{fp}. We use the term V_{n} to describe uncorrelated noise sources that add to the measured variance, e.g. electronic noise. Noise that is initially on the probe beam or noise sources that affect the probe beam at any point in the experiment (e.g. mechanical cavity resonances or an unstable cavity lock) are more comprehensive to describe and would overcomplicate the calculations shown here. We therefore neglect these noise terms but want to empathize that our approach is not immune to this type of noise. However, we elaborate on this in Sec. 5 and extend our idea to suppress these noise sources in Sec. 5.1.

2.2. Frequency up-shifting the signal

Typical noise sources occur primarily at LFs (<10 MHz). To circumvent the noise $V_{\mathrm{n}}(\omega)$, we measure our signal at HFs. Therefore, we extend our setup according to Fig. 2. A PM at HF ($\Omega \gg \omega_{\mathrm{s}}$) is imprinted by an electro-optic modulator (EOM) on the input field $\hat{A}_{\mathrm{in}}$, before the field enters the cavity. To maximize the transmission of the modulation sidebands, the modulation frequency Ω should correspond to the FSR of the FP cavity ($\Omega = \mathrm{FSR}_{\mathrm{fp}} = 1/\tau_{\mathrm{fp}}$).

Again, we assume a small modulation index β and use the Bessel approximation from Eq. (3). For the fluctuating part we get in frequency domain for the new input field

$$\delta\tilde{A}_{\mathrm{in}}(\omega) = \big(\delta\tilde{A}_{\mathrm{mod}}(\omega) + \frac{\beta}{2}\bar{A}_{\mathrm{mod}}(\tilde{\delta}_{\omega-\Omega} - \tilde{\delta}_{\omega+\Omega})\big)\exp(i\theta), \tag{12}$$

where $\tilde{A}_{\mathrm{mod}}$ corresponds to the field before the EOM. Here, we have dropped the $d\tilde{\delta}\tilde{A}$ terms assuming $d\tilde{\delta}\tilde{A} \ll d\bar{a}_{\mathrm{fp}}$. Then, the output variances of the cavity can be calculated analogously to

Optics EXPRESS

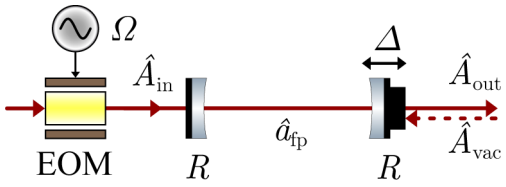

Fig. 2. Schematic of the length modulated FP cavity, with a phase modulated input field.

Sec. 2.1 yielding

$$V^{+}_{\mathrm{fp,pm}}(\omega) = V^{+}_{\mathrm{fp}}(\omega) + \left|\frac{\bar{A}_{\mathrm{mod}} dT\beta}{2(\exp(i\tau_{\mathrm{fp}}\omega) - R)}\right|^2 \times \left|(\delta_{\omega+\Omega-\omega_{\mathrm{s}}} + \delta_{\omega-\Omega+\omega_{\mathrm{s}}} - \delta_{\omega+\Omega+\omega_{\mathrm{s}}} - \delta_{\omega-\Omega-\omega_{\mathrm{s}}})\right|^2, \tag{13}$$

$$V^{-}_{\mathrm{fp,pm}}(\omega) = V^{-}_{\mathrm{fp}}(\omega) + \left|\frac{i\bar{A}_{\mathrm{mod}} T\beta}{\exp(i\tau_{\mathrm{fp}}\omega) - R}(\delta_{\omega+\Omega} - \delta_{\omega-\Omega})\right|^2 \tag{14}$$

where $V^{\pm}_{\mathrm{fp}}$ corresponds to the results from the previous section derived in Eqs. (8) and (9). The terms oscillating with $\omega \pm \omega_{\mathrm{s}}$ and $\omega \pm \Omega$ can be only seen in the phase quadrature V^{-}. The intermodulation terms oscillating with $\omega \pm \Omega \pm \omega_{\mathrm{s}}$ can be detected only in the output amplitude quadrature V^{+}, which is an important result. This result means that the cavity length modulation can also be resolved at HFs. External noise V_{n}, introduced in Eqs. (8) and (9) may still couple into the measurement. However, we can assume that there is negligible noise at hundreds of MHz.

Fundamentally, this measurement will be limited by the shot noise when technical noise sources on the probe beam are suppressed sufficiently. The relative shot noise level might be reduced by increasing the used laser power. However, this is often only possible in the limits of available and permissible power.

2.3. *High-frequency phase modulated squeezing*

One approach to further reduce noise and thereby improve the shot-noise-limited SNR is the usage of a squeezed probe field. In the following section we explain how such a field is generated and how its variances can be derived. The following calculations were similarly done for an unmodulated seed in [25].

We consider a singly resonant OPO that is operating below threshold at the fundamental frequency ω_0 as shown in Fig. 3. For simplification, we assume a cavity consisting of a partially reflective (PR) input mirror with $R_1 < 1$, a highly reflective (HR) mirror with $R_2 \approx 1$ and an ideal non-lossy mirror $R_3 = 1$ surrounding a non-linear $\chi^{(2)}$ medium. It is convenient to include the

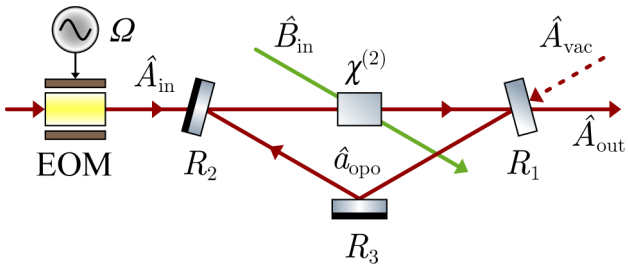

Fig. 3. Schematic of an OPO with a phase modulated seed as input.

Optics EXPRESS

effect of all intra-cavity losses in the reflectance of mirror 2. The nonlinear medium is pumped with the field $\hat{B}_{\text{in}}$ at the second harmonic frequency $\omega_{\text{pump}} = 2\omega_0$. The cavity round-trip time is τ_{opo} and, ideally, should be identical to the round-trip time in the FP cavity ($\text{FSR}_{\text{opo}} = \text{FSR}_{\text{fp}}$). A vacuum field $\hat{A}_{\text{vac}}$ is impinging on mirror 1 and the phase modulated seed field $\hat{A}_{\text{in}}$, identical to Eq. (12), is sent into the cavity on mirror 2. We are dealing with a single mode as we do not discriminate in frequency between the upper and lower sidebands. Thus we assume a single-mode interaction Hamiltonian with an undepleted pump field:

$$\mathcal{H} = \frac{i\hbar\chi}{2}\left(a^2 - a^{\dagger 2}\right). \tag{15}$$

As in subsections 2.1 and 2.2, the fundamental cavity mode $\hat{a}_{\text{opo}}$ after a single cavity round-trip with round-trip time τ_{opo} can be expressed on resonance by

$$\begin{aligned}\hat{a}_{\text{opo}}(t+\tau_{\text{opo}}) = &-\chi\tau_{\text{opo}}\hat{a}^{\dagger}_{\text{opo}}(t) + \sqrt{R_1R_2}\hat{a}_{\text{opo}}(t)\\ &+ \sqrt{R_1T_2\tau_{\text{opo}}}\hat{A}_{\text{in}}(t) + \sqrt{T_1\tau_{\text{opo}}}\hat{A}_{\text{vac}}(t).\end{aligned} \tag{16}$$

The solution for the fluctuating part $\delta\tilde{a}(\omega)_{\text{opo}}$ of the intra-cavity field in frequency domain can be computed similarly as above. Since the OPO is seeded with a phase modulated field, $\delta\tilde{A}_{\text{in}}$ is defined as in Eq. (12). To derive the desired fluctuations for the output field of the OPO, the boundary condition

$$\delta\tilde{A}_{\text{out,opo}} = \sqrt{T_1/\tau_{\text{opo}}}\delta\tilde{a}_{\text{opo}} - \sqrt{R_1}\delta\tilde{A}_{\text{vac}} \tag{17}$$

needs to be applied. We can now use $\delta\tilde{A}_{\text{out,opo}}$ for the OPO's output to substitute the FP cavity's input $\delta\hat{A}_{\text{in}}$ in Eq. (5). Then, the output variances of the FP cavity can be computed similarly to Eqs. (8) and (9)

$$V^{\pm}_{\text{fp}}(\omega) = V^{\pm}_{\text{cav}}(\omega) + \left|C^{\pm}(\omega)\right|^2 + V^{\pm}_{\text{n}}, \tag{18}$$

but become rather complex. The variance $V^{\pm}_{\text{cav}}$ is specified as

$$\begin{aligned}V^{\pm}_{\text{cav}} = &\left|A(\omega)\Big(-\sqrt{R} + \frac{T_1}{\exp(i\tau_{\text{fp}}\omega) - \sqrt{R_1R_2} \pm \tau_{\text{opo}}\chi}\Big) + B(\omega)\right|^2 V^{\pm}_{\text{vac}}(\omega)\\ &+ \left|\frac{\sqrt{R_1T_1T_2}T}{(\exp(i\tau_{\text{fp}}\omega)) - R)(\exp(i\tau_{\text{fp}}\omega) - \sqrt{R_1R_2} \pm \tau_{\text{opo}}\chi)}\right|^2 V^{\pm}_{\text{in}}(\omega).\end{aligned} \tag{19}$$

It shows how the variances of the impinging vacua and the seed are transformed by the two cavities and thus defines the shot noise level. In fact, it is important to take a closer look onto C^+. The situation is similar as before in Eqs. (13) and (14). C^+ represents the intermodulation sidebands we are interested in. We find

$$\begin{aligned}C^{+}(\omega) = &\frac{\bar{A}_{\text{mod}}dT\beta\sqrt{R_1T_1T_2}}{2(\exp(i\tau_{\text{fp}}\omega) - R)(\exp(i\tau_{\text{opo}}) - \sqrt{R_1R_2} - \tau_{\text{opo}}\chi)}\\ &\times(\delta_{\omega+\Omega-\omega_{\text{s}}} + \delta_{\omega-\Omega+\omega_{\text{s}}} - \delta_{\omega+\Omega+\omega_{\text{s}}} - \delta_{\omega-\Omega-\omega_{\text{s}}}).\end{aligned} \tag{20}$$

The sidebands oscillating with $\omega \pm \omega_{\text{s}}$ and $\omega \pm \Omega$ can be found in $C^-(\omega)$:

$$\begin{aligned}C^{-}(\omega) = &\frac{i\bar{A}_{\text{mod}}T\beta\sqrt{R_1T_1T_2}}{(\exp(i\tau_{\text{fp}}\omega) - R)(\exp(i\tau_{\text{opo}}) - \sqrt{R_1R_2} - \tau_{\text{opo}}\chi)}(\delta_{\omega+\Omega} - \delta_{\omega-\Omega})\\ &+ \frac{i\bar{a}_{\text{fp}}d\sqrt{T/\tau_{\text{fp}}}}{\exp(i\tau_{\text{fp}}\omega) - R}(\delta_{\omega+\Omega} - \delta_{\omega-\Omega}).\end{aligned} \tag{21}$$

Choosing amplitude quadrature squeezing by setting the phase of the seed $\theta = 0$ in Eq. (12), we achieve a reduced noise floor in the amplitude quadrature and an increased noise floor in

Optics EXPRESS

the phase quadrature in Eq. (18). Thereby, we improve the SNR measuring the cavity length modulation.

The variance in Eq. (18) is only an idealization. If the field is measured with a homodyne detector (HD) to access the phase quadrature, phase fluctuations between the signal and the local oscillator (LO) need to be taken into account. For small standard deviations of the normally distributed phase fluctuations, phase jitter with a root mean square of ϕ will affect the detection angle at the HD. Including the total efficiency η and thus optical loss, we can write the measured variances behind the FP cavity as [38]

$$V^{\pm}_{\mathrm{fp,det}}(\omega) = \eta\left(V^{\pm}_{\mathrm{fp}}(\omega)\cos^2(\phi) + V^{\mp}_{\mathrm{fp}}(\omega)\sin^2(\phi)\right) + (1-\eta). \tag{22}$$

Hence, the output variance will be a mixture of the amplitude and phase quadrature V^+ and V^-. In consequence, the squeezing level will be reduced and all existent sidebands, to some degree, will be visible in both measured variances. We will use Eq. (22) for fitting our experimental data in Sec. 4. However, we will first present our experimental setup in the next section.

3. Experimental setup

Our experimental setup shown in Fig. 4 can be divided into three subsystems. The first part is the preparation stage and consists of the OPO, our non-classical light source. Here, our probe beam is generated which is a phase modulated but amplitude quadrature squeezed field. This field is sent into our second subsystem, the FP cavity. Here, we apply a cavity length modulation to mimic a spectroscopic signal. Finally, our third subsystem consists of a balanced HD where we resolve the length modulation signal in a squeezed sub-shot-noise floor at HFs.

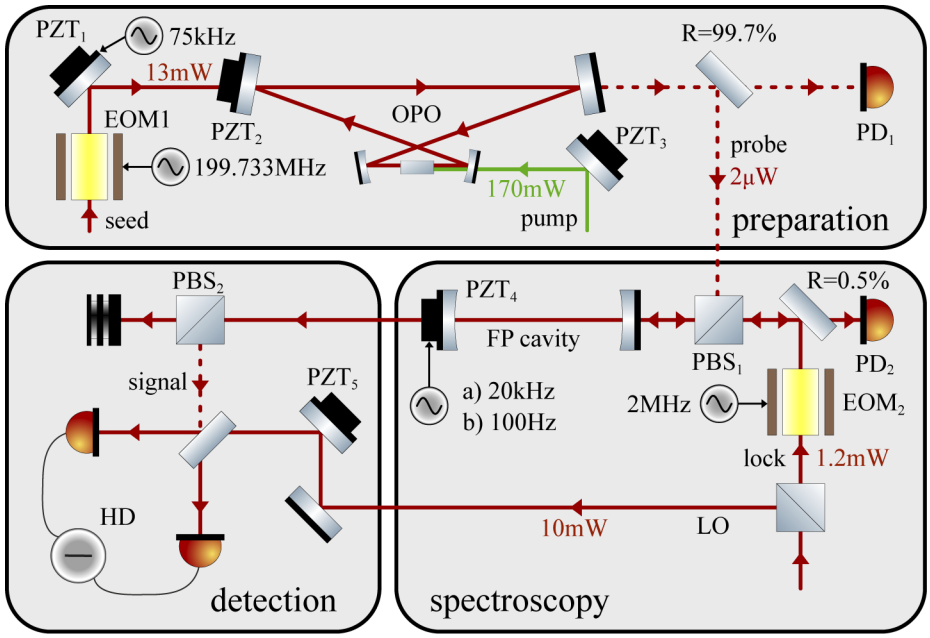

Fig. 4. The experimental setup consisting of the three subsystems: squeezed state preparation, spectroscopy and homodyne detection.

3.1. *Non-classical light source*

Our non-classical light source consists of a sub-threshold OPO, shown in the upper block of Fig. 4. In this block, all shown laser fields are s-polarized. The OPO has a comparably long

Optics EXPRESS

round-trip length of $L_{opo} \approx 1.5$m. This leads to a relatively small FSR of 199.66 MHz. Two curved mirrors with radius of curvature of −100 mm create a cavity eigenmode with beam waist of 25.6 µm in the crystal. The OPO is seeded with a phase modulated classical laser field through an HR mirror (transmission $T = 0.01\%$) that is attached to a piezoelectric element (PZT_2) from the left side. The PM frequency of 199.733 MHz is chosen to match the FSR of the OPO and, in particular, of the FP cavity (see Sec. 3.2 and Table 1). This ensures that the PM sidebands are transmitted by the two cavities. The singly-resonant OPO cavity is held on resonance with PZT_2 for 1064 nm using a field in counter-propagating direction of the cavity. This field is not depicted in the Fig. 4 for simplicity. The 1mm × 2mm × 10mm nonlinear PPKTP crystal is pumped with 170 mW at 532 nm. To reach a stable production of amplitude quadrature squeezing in the probe beam, the squeezing angle needs to be locked: First, we modulate the phase of the seed with 73 kHz, by dithering the PZT_1 attached to a steering mirror. Second, 0.3 % of the probe's power are detected on the photodiode (PD_1) behind a PR mirror. Then, the detected signal is demodulated to generate an error signal which is sent back to PZT_3. The full characterization of our non-classical light source ("squeezing comb") and its performance is given in detail in a publication currently under preparation. The most important parameters characterizing the OPO are given in Table 1.

Table 1. Important parameters of OPO and FP cavity.

OPO	Value	Error	Unit
linewidth (FWHM)	4.5	±0.1	MHz
FSR	199.66	±0.01	MHz
pump power	170	±12	mW
escape efficiency	97	±1	%
FP cavity	**Value**	**Error**	**Unit**
linewidth (FWHM)	200	±7	kHz
FSR	199.733	±0.01	MHz
finesse	998	±33	
round-trip-loss	90	±10	ppm

3.2. *Fabry-Pérot cavity for spectroscopy*

The second subsystem is shown in the right bottom block of Fig. 4 including the FP cavity as the spectroscopic device. In the FP cavity the artificial signal is created by actuating PZT_4 which corresponds to a cavity length modulation. The FP cavity consists of two PR mirrors ($R = 99.69\%$, ROC = 2m) attached to an aluminum spacer in a distance of roughly 37.5 cm. The intra-cavity loss per round-trip is 90 ppm and the exact FSR of the FP cavity is 199.733 MHz. Hence, the cavity finesse is 998 and the linewidth at the full width at half maximum (FWHM) is 200 kHz. The output mirror is attached on PZT_4 to modify the cavity length.

We stabilize the FP cavity with the p-polarized lock beam, so that it is resonant for our s-polarized probe beam. This is possible because the cavity is radially symmetric and therefore degenerated for s- and p-polarization. The lock field is phase modulated with EOM_2 at 2 MHz and sent into the FP cavity. The part that is reflected is detected on PD_2, demodulated, low-pass-filtered and fed back to PZT_4 [39]. The s-polarized amplitude quadrature squeezed probe field coming from the OPO is reflected at PBS_1 and it is also injected into the resonant FP cavity. PBS_2 is used to separate the lock field from the signal field in transmission of the FP cavity.

In our approach we show that small phase signals created in the FP cavity can be resolved by the use of amplitude quadrature squeezing. In order to generate these signals, we can apply tiny length modulations with a) 20 kHz (amplitude (9.8±1.0) pm) and b) 100 Hz (amplitude

Optics EXPRESS

(25.4±1.0) pm) on PZT_4. The corresponding PZT amplitudes are obtained from the fits in Fig. 6, see Sec. 4.2, via the fitting parameter d. Both modulation frequencies are smaller than the linewidth of the FP cavity. We can easily modify the modulation strength by changing the voltage applied to the PZT_4. We summarize all important parameters in Table 1.

3.3. Balanced homodyne detection

The detection stage is the third subystem of our setup, depicted in the bottom left corner of Fig. 4. In this stage we measure the phase and amplitude quadratures of the signal field. We use a balanced HD where the signal is interfered with the s-polarized LO. The detector has a low-noise AC output to access the signal's fluctuations. The detector's DC output is used to lock the detection angle. The relative phase information between LO and signal is encoded in the beat signal. The DC slope can be taken as error signal to lock the detection angle on phase quadrature. For an amplitude quadrature readout, we need to stabilize at an interference maximum. Therefore, we demodulate the signal at 73 kHz and low-pass filter it to obtain the corresponding error signal. In both cases, the error signal is applied to PZT_5. In the next section we present measurements of the signal's phase and the amplitude quadratures.

4. Results

In this section, we present, characterize and discuss our measurements. First, we quantify the performance of our non-classical light source after integration into the setup, behind the FP cavity. Second, we detect two different cavity length modulation signals. Finally, we discuss our approach and give a brief outlook.

4.1. Squeezing performance behind the FP cavity

We measured the noise spectrum of our amplitude quadrature squeezed state in transmission of the FP cavity with an unmodulated probe field (EOM_1 turned off in Fig. 4). For a full characterization, we measured squeezing (sqz) in the amplitude quadrature (blue trace) and anti-squeezing in the phase quadrature (red trace) in Fig. 5. The measurements are normalized to the shot noise which is measured classically when the pump of the OPO is turned off. Thus, the 0 dB level corresponds to the quantum shot noise limit. All presented measurements in this section are taken with a Keysight N9020a MXA signal analyzer.

Table 2. Fitting parameters plugged in Eq. (22) for creating the fits in Fig. 5.

Parameter	Value
R_1	90 %
R_2	99.99 %
$\mathrm{FSR_{opo}}$	199.66 MHz
χ	7.39 MHz
R	99.69 %
$\mathrm{FSR_{fp}}$	199.733 MHz
$\bar{A}_{\mathrm{mod}}$	0
η	86 %
ϕ	38 mrad

On cavity resonance, we detected 6.7 dB squeezing and 14.7 dB anti-squeezing after subtracting the electronic DN, which is approximately 14.2 dB below the shot noise. For comparison, without the FP cavity 8.2 dB of squeezing and 15.1 dB of anti-squeezing were measured. This vertical

Optics EXPRESS

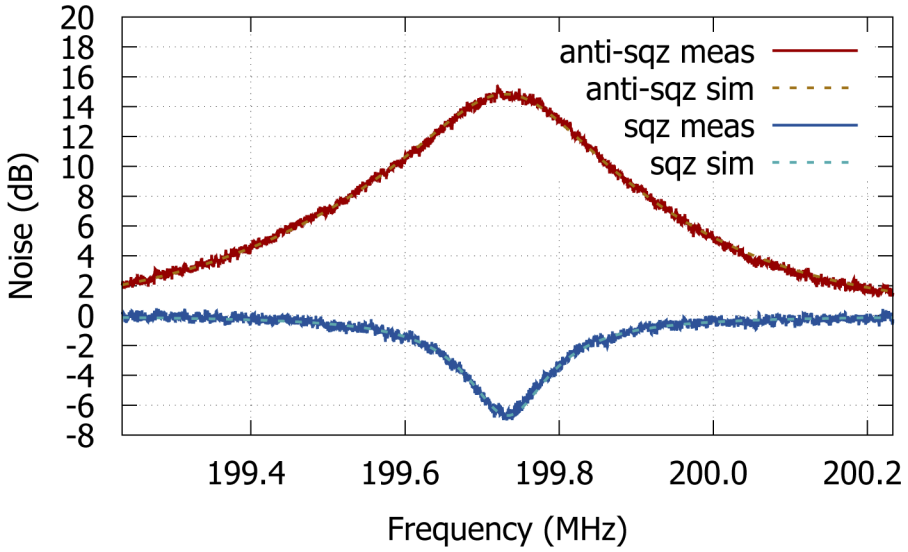

Fig. 5. Spectrum of the amplitude quadrature squeezed state behind the FP cavity. The simulation was obtained with Eq. (22). For the measurement, the detection angle is locked onto amplitude quadrature to observe squeezing and onto phase quadrature to see anti-squeezing. The spectrum was taken around the center frequency of 199.733 MHz which is equal to the FSR of the FP cavity, see Table 2. The dark noise (DN) of the HD was subtracted from the raw data. Further, it was normalized to the shot noise level, which was 14.2 dB above the dark noise (DN). Span 1 MHz, resolution bandwidth (RBW) 5.1 kHz, video bandwidth (VBW) 20 Hz, avg 10. For comparison, without the FP cavity 8.2 dB of squeezing and 15.1 dB of anti-squeezing with a phase noise of 30 mrad were measured.

asymmetry depends on the amount of optical loss and phase noise [17,40] and can be explained by Eq. (22). The FSRs of the OPO and the FP cavity were not perfectly matched and differed by 73 kHz (see Table 1), which corresponds to an optical round-trip length difference of 55 µm. Notwithstanding, the maximal squeezing degradation due to this mismatch is only 0.01 dB.

Our measured data agrees well with our theoretical model from Eq. (22), fitted by the dashed traces in Fig. 5. Table 2 gives an overview of the fitting parameters. The most relevant parameters to characterize the performance are the total efficiency $\eta = 86\%$ and the root mean square phase noise $\phi = 38$mrad. For comparison, without the FP cavity 30 mrad of phase noise was measured. In further measurements we determined the composition of η. The escape efficiency of our OPO was $\eta_{\mathrm{esc}} = 97 \pm 1\%$. The total propagation efficiency including all optics and FP cavity was $\eta_{\mathrm{prop}} = 94 \pm 1\%$. The efficiency of the detection process is determined by the homodyne visibility $\eta_{\mathrm{vis}} = 98.5 \pm 0.5\%$. Thus the quantum efficiency $\eta_{\mathrm{qe}} = 96 \pm 1\%$ of the HD was obtained as in [17], by using $\eta = \eta_{\mathrm{esc}}\eta_{\mathrm{prop}}\eta_{\mathrm{vis}}\eta_{\mathrm{qe}}$.

The linewidths of squeezing and anti-squeezing become unequal behind the FP cavity, see again Fig. 5. This linewidth asymmetry can be explained by the smaller linewidth of the FP cavity compared to the OPO. Frequency contributions outside of the linewidth of the FP cavity experience a significantly higher loss which degrades the squeezing far more than the anti-squeezing, see Eq. (22). To our knowledge, this created asymmetry has not been shown in previous publications.

Optics EXPRESS

4.2. Measuring a cavity length modulation

We turned on the PM applied on EOM_1 to acquire the length modulation signals of the FP cavity at the first FSR. As before, we generate an amplitude quadrature squeezed state, but additionally it is phase modulated at 199.733 MHz. The frequency is tuned to match the FSR of the FP cavity. We first demonstrate the general feasibility of our method by injecting a kHz cavity length modulation. Since external noise often increases with decreasing frequency, we secondly push the experiment to the LF limit. In each case we compare our results with the classical (class) case which corresponds to shot noise, when the pump of the OPO is turned off.

First, we apply a cavity length modulation at 20 kHz with an amplitude of 9.8 pm and measure the output variances plotted in Fig. 6(a)). We see two peaks in a frequency distance of 20 kHz to the EOM peak corresponding to the length modulation. The peaks maxima are located 2.9 dB below shot noise in the 5.7 dB squeezed noise floor. Again, the turquoise dashed trace was plotted with Eq. (22) and agrees well with the measured data. For comparison, we repeated the measurement for the classical case when the OPO's pump is blocked. This measurement is shown in red in Fig. 6. Here, we effectively cannot reveal the cavity length modulation. Our simulation (dashed orange trace) predicts a peak size of 0.08 dB above shot noise which would require significantly more averaging to resolve experimentally. In conclusion we see an effective SNR improvement of 5.7 dB. The parameters needed for the simulation can be found in Table 3. To plot the Dirac delta-like function from Eq. (22), we used a normalized Gaussian distribution, with

$$\tilde{\delta}_\omega = \tilde{\delta}(\omega) = \exp\left(-\frac{\omega^2}{2\sigma^2}\right) \quad \text{and} \quad \sigma = \text{RBW}. \tag{23}$$

Table 3. Parameters plugged in Eq. (22) for creating the fits in Fig. 6. Missing parameters are identical to Table 2.

Parameter	a)	b)
ω_s	20 kHz	100 Hz
Ω	199.733 MHz	
$\bar{A}_{\text{mod}}$	$3.3\times10^6\ \sqrt{\text{Hz}}$	
β	3.3×10^{-5}	9.1×10^{-5}
d	5.8×10^{-5}	1.5×10^{-4}
ϕ	49 mrad	51 mrad

Finally, we demonstrate that our method can even resolve sub-kHz signals, that are presumably more affected by LF external noise. We have chosen a cavity length modulation of 100 Hz with an amplitude of 25.4 pm. The measured spectrum can be found in Fig. 6(b). We get similar results as in a): the two peaks originating from the length modulation have a maximum of 2.8 dB below shot noise in a 6.0 dB squeezed noise floor. Thereby, we improved the signal to noise ratio by 6.0 dB at this frequency compared to the classical case, where the length modulation cannot be effectively resolved. Again, the experimental data can be well fitted with our derived theory, shown by the dashed traces.

For the given set of seed power and modulation index of the EOM, we could resolve displacement signals with an amplitude down to 4 pm at 20 kHz and 14 pm at 100 Hz with signals 1 dB larger than the squeezed noise floor.

Optics EXPRESS

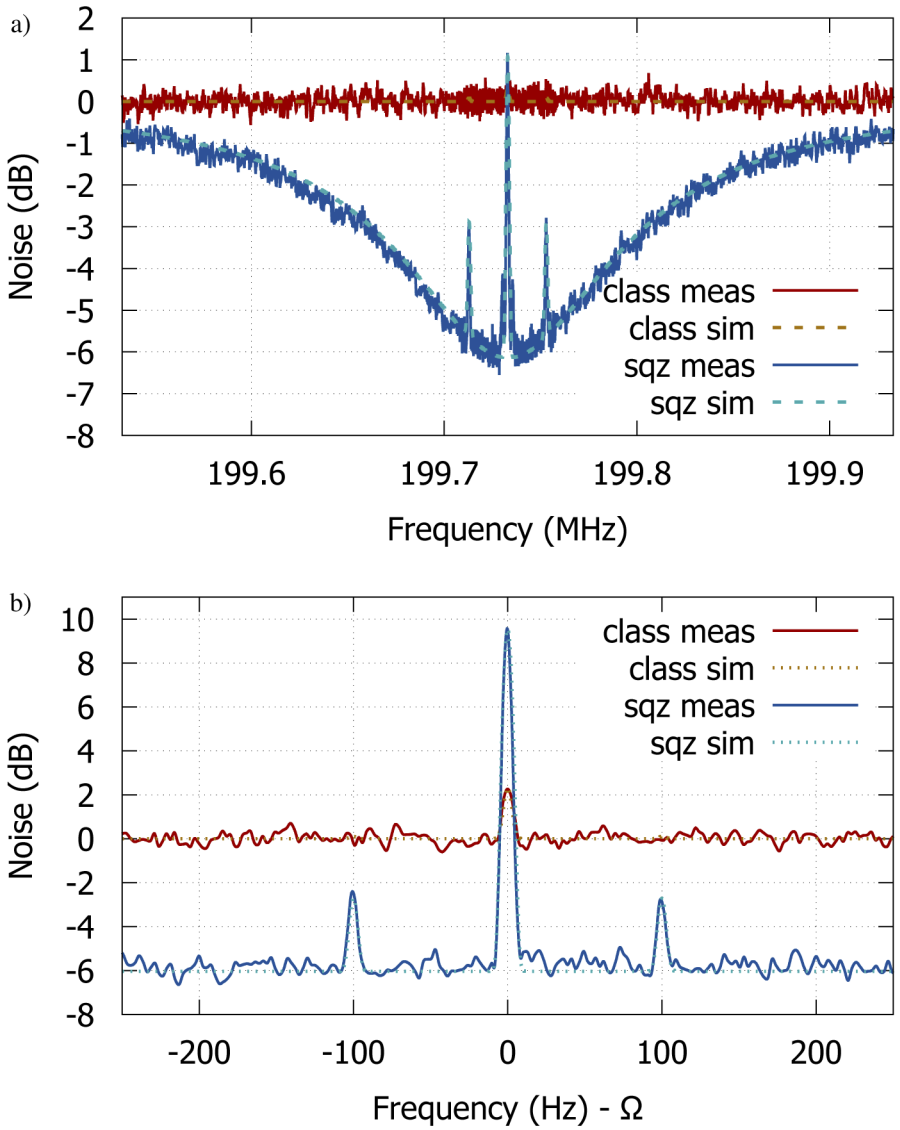

Fig. 6. Resolved cavity length modulation signals applied at a) 20 kHz and b) 100 Hz in the squeezed noise floor. The center frequency corresponds to Ω = 199.733MHz. The peaks located at this frequency are related to the PM sideband of the EOM and mainly originate from phase quadrature to amplitude quadrature coupling via phase noise, see Eq. (22). For the squeezed case, the peaks are enhanced compared to the classical case since the phase quadrature is amplified due to anti-squeezing. In a), the peaks at a distance of 2.6 kHz to the center peak originate from a FP cavity resonance. Parameters of the signal analyzer: a) two distinct measurements: span 400 kHz: RBW 1 kHz, VBW 10 Hz, avg 50; span 50 kHz: RBW 5.1 kHz, VBW 20 Hz, avg 10 (DN and SN avg 50), b) span 500 Hz: RBW 5.1 Hz, VBW 1 Hz, avg 300.

Optics EXPRESS

5. Discussion

We have demonstrated that our method is capable of resolving tiny signals otherwise masked by quantum shot noise, by using HF squeezed light and sophisticated modulation techniques. In comparison to previous spectroscopic experiments in literature employing base-band squeezed light [28–30], we have significantly improved the squeezing level while sending our probe beam through an optical resonator.

In contrast to base-band experiments, we need significantly less effort locking the squeezing angle. Even though it is possible to control the squeezing angle using a noise dither technique without a carrier [23,41], more stable locks can be achieved using bright optical fields that co-propagate with the squeezed vacuum [42,43]. However, for base-band measurements these fields need to be frequency shifted [24] to avoid excess noise caused by the LF laser noise. In our case of measuring at HFs, we can avoid this effort and use our seed field to control the squeezing angle.

Our experiment is sensitive to some types of noise and immune to others. It is not immune to any disturbances that act as phase or amplitude noise coupling into our laser field, similar to [30]. These disturbances cannot be differentiated from the cavity modulation signal we want to detect. This kind of noise might be caused by e.g. temperature fluctuations or vibrations that are affecting the stability of the laser resonator or optical components. These sources have in common that they will also appear around the EOM sideband at HF, since they all experience the modulation process. Contrariwise, any noise sources coupling into the measurement that do *not* add coherently on our laser field, are circumvented because they do not occur on the EOM sideband at HF. Those noise sources are predominantly at LFs. Examples for these kind of noises are electric or post processing noise, incoherent stray light like ambient light or infrared thermal radiation.

Our demonstrated approach has a number of advantages. Technical laser noise typically occurs at frequency ranges from Hz to 100 kHz and drops off for higher frequencies ($\sim$ MHz). Therefore our LO does not exhibit technical noise around 200 MHz and is thus shot noise limited. Imperfections like a non-ideal common-mode rejection at the HD will have a much lower impact than at LF, where technical noise is present. Since our high-frequency squeezer is built in a bow-tie topology, back-scattered light is significantly suppressed in comparison to linear squeezers [44]. Furthermore, in our case of perfect frequency matching ($\mathrm{FSR_{fp}} = \Omega$) all PM sidebands are transmitted by the cavity symmetrically in frequency. Therefore all sidebands experience frequency noise identically, such that frequency-to-amplitude noise coupling in the cavity is strongly suppressed. This feature is often referred to as *laser frequency noise immunity* [45] and is used e.g. in NICE-OHMS [32].

Our technique is not fundamentally limited to the detection of preferably LF signals. However, to resolve the cavity length modulation sidebands with high precision, two technical requirements need to be fulfilled: The spectrum analyzer needs a sufficiently high resolution, and the EOM must produce sufficient narrowband and stable sidebands. We used a network analyzer [Keysight E5061B] to generate the signal at 199.733 MHz. The generated signal has a measured bandwidth of <1Hz, which is limited by the RBW of our spectrum analyzer. For further improvement towards measurements at lower cavity length modulation frequencies a better RBW is hence required.

5.1. Outlook

With our approach we have demonstrated the detection of small sub-shot-noise phase signals. In order to measure amplitude signals, merely the detection angle at the HD needs to be adjusted for readout of the orthogonal quadrature. For an improved common-mode rejection of phase fluctuations on LO and probe beam the two beams have to co-propagate in the FP cavity. This will lead to a significant reduction of phase noise imprinted by the FP cavity on the probe beam. To

Optics EXPRESS

achieve this, the LO has to be orthogonally polarized to the probe beam. The common-mode phase fluctuations do not affect our final measurement in transmission, where the probe's amplitude quadrature can be measured with a polarization based HD scheme [46].

As discussed before, our approach is still sensitive to technical noise sources that couple into our probe beam. We therefore propose to implement the spectroscopic FP cavity in one arm of a Michelson interferometer. A HF phase modulated field similar to our seed is coupled into the interferometer's input port. The HF squeezed field is sent into the interferometer's output port. For a specific interferometer design, the LF cavity length modulation sidebands will exit the interferometer at HF in the squeezed noise floor and will interfere with a coherent field at DC. This technique is similar to a gravitational wave detector operated with DC readout [47]. To reduce technical noise on the probe beam this is a promising approach which deserves further investigation.

6. Conclusion

We have presented a new method to significantly improve the signal-to-shot-noise level in high-precision spectroscopic measurements without increasing the laser power. Our approach circumvents technical noise sources such as low-frequency detection noise by applying a high-frequency PM. Additionally, the shot noise of the probe beam is squeezed by a sub-threshold OPO. With this prepared phase modulated, amplitude quadrature squeezed probe, we demonstrated a sub-shot-noise limited detection of small spectroscopic phase signals. In our experiment, we were able to resolve tiny cavity length modulations at 20 kHz (100 Hz) on a squeezed noise floor of 5.7 dB (6.0 dB). The derived theory confirms the measurements very well.

Our approach is interesting for spectroscopic applications, e.g. for FMS [33]. Experiments where the probe under investigation (e.g. a gas) may set a certain laser power limit can also benefit from our technique, since it allows to increase the SNR without the need for higher laser power.

Funding. Deutsche Forschungsgemeinschaft (Excellence PhoenixD (EXC 2122, Excellence QuantumFrontiers (EXC 2123, Project ID 390833453), Project ID 390837967)).

Acknowledgments. The authors wish to thank Charles Harb for productive discussions.

Disclosures. The authors declare no conflicts of interest.

References

1. B. P. T. D. e. a. Abbott, "Observation of Gravitational Waves from a Binary Black Hole Merger," Phys. Rev. Lett. **116**(6), 061102 (2016).
2. G. C. Bjorklund, "Frequency-modulation spectroscopy: a new method for measuring weak absorptions and dispersions," Opt. Lett. **5**(1), 15–17 (1980).
3. J. J. Scherer, D. Voelkel, D. J. Rakestraw, J. B. Paul, C. P. Collier, R. J. Saykally, and A. O'Keefe, "Infrared cavity ringdown laser absorption spectroscopy (IR-CRLAS)," Chem. Phys. Lett. **245**(2-3), 273–280 (1995).
4. P. Kwee, B. Willke, and K. Danzmann, "Shot-noise-limited laser power stabilization with a high-power photodiode array," Opt. Lett. **34**(19), 2912–2914 (2009).
5. J. Junker, P. Oppermann, and B. Willke, "Shot-noise-limited laser power stabilization for the AEI 10m Prototype interferometer," Opt. Lett. **42**(4), 755 (2017).
6. H. Vahlbruch, D. Wilken, M. Mehmet, and B. Willke, "Laser power stabilization beyond the shot noise limit using squeezed light," Phys. Rev. Lett. **121**(17), 173601 (2018).
7. C. Gardiner and P. Zoller, *Quantum Noise - A Handbook of Markovian and Non-Markovian Quantum Stochastic Methods with Applications to Quantum Optics* (Springer Science & Business Media, Berlin Heidelberg, 2004).
8. M. L. Denton, M. S. Foltz, L. E. Estlack, D. J. Stolarski, G. D. Noojin, R. J. Thomas, D. Eikum, and B. A. Rockwell, "Damage thresholds for exposure to NIR and blue lasers in an in vitro RPE cell system," Invest. Ophthalmol. Visual Sci. **47**(7), 3065–3073 (2006).
9. C. A. Casacio, L. S. Madsen, A. Terrasson, M. Waleed, K. Barnscheidt, B. Hage, M. A. Taylor, and W. P. Bowen, "Quantum correlations overcome the photodamage limits of light microscopy," arXiv:2004.00178 [physics.optics], https://arxiv.org/abs/2004.00178 (2020).
10. R. A. e. a. J. Abadie and B. P. Abbott, "Predictions for the rates of compact binary coalescences observable by ground-based gravitational-wave detectors," Classical Quantum Gravity **27**(17), 173001 (2010).

Optics EXPRESS

11. H.-A. Bachor and T. C. Ralph, *A Guide to Experiments in Quantum Optics* (Wiley, New York, 2004).
12. U. L. Andersen, T. Gehring, C. Marquardt, and G. Leuchs, "30 years of squeezed light generation," Phys. Scr. **91**(5), 053001 (2016).
13. J. Lough, E. Schreiber, F. Bergamin, H. Grote, M. Mehmet, H. Vahlbruch, C. Affeldt, M. Brinkmann, A. Bisht, V. Kringel, H. Luck, N. Mukund, S. Nadji, B. Sorazu, K. Strain, M. Weinert, and K. Danzmann, "First demonstration of 6 db quantum noise reduction in a kilometer scale gravitational wave observatory," arXiv:2005.10292 [physics.ins-det], https://arxiv.org/abs/2005.10292 (2020).
14. A. L. e. a. Acernese F. and M. Agathos, "Increasing the astrophysical reach of the advanced virgo detector via the application of squeezed vacuum states of light," Phys. Rev. Lett. **123**(23), 231108 (2019).
15. K. N. e. a. Tse M. and Yu Haocun, "Quantum-enhanced advanced ligo detectors in the era of gravitational-wave astronomy," Phys. Rev. Lett. **123**(23), 231107 (2019).
16. R. E. Slusher, L. W. Hollberg, B. Yurke, J. C. Mertz, and J. F. Valley, "Observation of squeezed states generated by four-wave mixing in an optical cavity," Phys. Rev. Lett. **55**(22), 2409–2412 (1985).
17. H. Vahlbruch, M. Mehmet, K. Danzmann, and R. Schnabel, "Detection of 15 db squeezed states of light and their application for the absolute calibration of photoelectric quantum efficiency," Phys. Rev. Lett. **117**(11), 110801 (2016).
18. N. C. Menicucci, P. van Loock, M. Gu, C. Weedbrook, T. C. Ralph, and M. A. Nielsen, "Universal quantum computation with continuous-variable cluster states," Phys. Rev. Lett. **97**(11), 110501 (2006).
19. N. Treps, U. Andersen, B. Buchler, P. K. Lam, A. Maître, H.-A. Bachor, and C. Fabre, "Surpassing the standard quantum limit for optical imaging using nonclassical multimode light," Phys. Rev. Lett. **88**(20), 203601 (2002).
20. M. I. Kolobov and C. Fabre, "Quantum limits on optical resolution," Phys. Rev. Lett. **85**(18), 3789–3792 (2000).
21. S. L. Braunstein and H. J. Kimble, "Teleportation of continuous quantum variables," Phys. Rev. Lett. **80**(4), 869–872 (1998).
22. A. Furusawa, J. L. Sørensen, S. L. Braunstein, C. A. Fuchs, H. J. Kimble, and E. S. Polzik, "Unconditional quantum teleportation," Science **282**(5389), 706–709 (1998).
23. K. McKenzie, N. Grosse, W. P. Bowen, S. E. Whitcomb, M. B. Gray, D. E. McClelland, and P. K. Lam, "Squeezing in the audio gravitational-wave detection band," Phys. Rev. Lett. **93**(16), 161105 (2004).
24. H. Vahlbruch, S. Chelkowski, B. Hage, A. Franzen, K. Danzmann, and R. Schnabel, "Coherent control of vacuum squeezing in the gravitational-wave detection band," Phys. Rev. Lett. **97**(1), 011101 (2006).
25. A. E. Dunlop, E. H. Huntington, C. C. Harb, and T. C. Ralph, "Generation of a frequency comb of squeezing in an optical parametric oscillator," Phys. Rev. A **73**(1), 013817 (2006).
26. R. J. Senior, G. N. Milford, J. Janousek, A. E. Dunlop, K. Wagner, H.-A. Bachor, T. C. Ralph, E. H. Huntington, and C. C. Harb, "Observation of a comb of optical squeezing over many gigahertz of bandwidth," Opt. Express **15**(9), 5310 (2007).
27. M. Heurs, J. G. Webb, A. E. Dunlop, C. C. Harb, T. C. Ralph, and E. H. Huntington, "Multiplexed communication over a high-speed quantum channel," Phys. Rev. A **81**(3), 032325 (2010).
28. N. P. Georgiades, E. S. Polzik, K. Edamatsu, H. J. Kimble, and A. S. Parkins, "Nonclassical excitation for atoms in a squeezed vacuum," Phys. Rev. Lett. **75**(19), 3426–3429 (1995).
29. V. G. Lucivero, R. Jiménez-Martínez, J. Kong, and M. W. Mitchell, "Squeezed-light spin noise spectroscopy," Phys. Rev. A **93**(5), 053802 (2016).
30. E. S. Polzik, J. Carri, and H. J. Kimble, "Spectroscopy with squeezed light," Phys. Rev. Lett. **68**(20), 3020–3023 (1992).
31. R. B. de Andrade, H. Kerdoncuff, K. Berg-Sørensen, T. Gehring, M. Lassen, and U. L. Andersen, "Quantum-enhanced continuous-wave stimulated raman scattering spectroscopy," Optica **7**(5), 470–475 (2020).
32. J. Ye, L.-S. Ma, and J. L. Hall, "Ultrasensitive detections in atomic and molecular physics: demonstration in molecular overtone spectroscopy," J. Opt. Soc. Am. B **15**(1), 6 (1998).
33. B. Yurke and E. A. Whittaker, "Squeezed-state-enhanced frequency-modulation spectroscopy," Opt. Lett. **12**(4), 236–238 (1987).
34. S. S. Brown, H. Stark, and A. R. Ravishankara, "Cavity ring-down spectroscopy for atmospheric trace gas detection: Application to the nitrate radical (NO3)," Appl. Phys. B **75**(2-3), 173–182 (2002).
35. B. A. Paldus, C. C. Harb, T. G. Spence, R. N. Zare, C. Gmachl, F. Capasso, D. L. Sivco, J. N. Baillargeon, A. L. Hutchinson, and A. Y. Cho, "Cavity ringdown spectroscopy using mid-infrared quantum-cascade lasers," Opt. Lett. **25**(9), 666 (2000).
36. M. J. Collett and C. W. Gardiner, "Squeezing of intracavity and traveling-wave light fields produced in parametric amplification," Phys. Rev. A **30**(3), 1386–1391 (1984).
37. R. J. Glauber, "The quantum theory of optical coherence," Phys. Rev. **130**(6), 2529–2539 (1963).
38. M. Mehmet, S. Ast, T. Eberle, S. Steinlechner, H. Vahlbruch, and R. Schnabel, "Squeezed light at 1550 nm with a quantum noise reduction of 12.3 db," Opt. Express **19**(25), 25763–25772 (2011).
39. R. W. P. Drever, J. L. Hall, F. V. Kowalski, J. Hough, G. M. Ford, A. J. Monley, and H. Ward, "Laser phase and frequency stabilization using an optical resonator," Appl. Phys. B **31**(2), 97–105 (1983).
40. Y. Takeno, M. Yukawa, H. Yonezawa, and A. Furusawa, "Observation of -9 dB quadrature squeezing with improvement of phase stability in homodyne measurement," Opt. Express **15**(7), 4321 (2007).
41. K. McKenzie, E. E. Mikhailov, K. Goda, P. K. Lam, N. Grosse, M. B. Gray, N. Mavalvala, and D. E. McClelland, "Quantum noise locking," J. Opt. B: Quantum Semiclassical Opt. **7**(10), S421–S428 (2005).

Optics EXPRESS

42. S. Chelkowski, H. Vahlbruch, B. Hage, A. Franzen, N. Lastzka, K. Danzmann, and R. Schnabel, "Experimental characterization of frequency-dependent squeezed light," Phys. Rev. A **71**(1), 013806 (2005).
43. R. Schnabel, W. Bowen, N. Treps, B. Buchler, T. Ralph, P. K. Lam, and H.-A. Bachor, "Optical experiments beyond the quantum limit: Squeezing, entanglement, and teleportation," Opt. Spectrosc. **94**(5), 651–665 (2003).
44. S. S. Y. Chua, M. S. Stefszky, C. M. Mow-Lowry, B. C. Buchler, S. Dwyer, D. A. Shaddock, P. K. Lam, and D. E. McClelland, "Backscatter tolerant squeezed light source for advanced gravitational-wave detectors," Opt. Lett. **36**(23), 4680–4682 (2011).
45. A. Foltynowicz, F. Schmidt, W. Ma, and O. Axner, "Noise-immune cavity-enhanced optical heterodyne molecular spectroscopy: Current status and future potential," Appl. Phys. B **92**(3), 313–326 (2008).
46. M. Heurs, I. R. Petersen, M. R. James, and E. H. Huntington, "Homodyne locking of a squeezer," Opt. Lett. **34**(16), 2465–2467 (2009).
47. S. Hild, H. Grote, J. Degallaix, S. Chelkowski, K. Danzmann, A. Freise, M. Hewitson, J. Hough, H. Luck, M. Prijatelj, K. A. Strain, J. R. Smith, and B. Willke, "DC-readout of a signal-recycled gravitational wave detector," Classical Quantum Gravity **26**(5), 055012 (2009).